 doi:10.1088/1742-6596/3124/1/012022

# Shadowgraphy of the plasma evolution around water micro-droplets irradiated by high-power laser pulses

**M. Beyer[1,2], Y. Azamoum[1,2], M. C. Nolte[1], G. A. Becker[1], M. B. Schwab[1,2], M. Hornung[1,2], M. Hellwing[1], T. Weickhardt[1] and M. C. Kaluza[1,2]**

[1] Institute of Optics and Quantum Electronics Jena, Max-Wien-Platz 1, 07743 Jena, Germany
[2] Helmholtz Institute Jena, Fröbelstieg 3, 07743 Jena, Germany

E-mail: `m.beyer@uni-jena.de`

**Abstract.** We investigate experimentally the plasma dynamics produced in a relativistic laser-water micro-droplet interaction using optical off-harmonic laser probe pulses. The laser pulses were focused onto water droplets (diameter 20 µm) to intensities of $4 \times 10^{19}\,\mathrm{W\,cm^{-2}}$. The plasma expansion process was probed in a temporal window between −4 ps and 260 ps after the arrival of the pump laser pulse. The strong light emission from the laser-generated plasma at the fundamental and second harmonic frequencies was suppressed in the probe images by spectrally filtering the light at the off-harmonic probe pulse's central wavelength. The plasma emission was further reduced by a polarization and a spatial filter (coronagraph). A detailed analysis of the shadowgraphy images allowed us to estimate the plasma expansion velocity of the front, $v_{\mathrm{front}} = 1.3\,\mathrm{\mu m\,ps^{-1}}$, and rear side, $v_{\mathrm{rear}} = 0.8\,\mathrm{\mu m\,ps^{-1}}$, at early times of the interaction. These values are in accordance with previously reported measurements of plasma expansion using liquid targets.

## 1. Introduction

The development of tools to measure the plasma generated during a relativistic laser-matter interaction is important to deepen the understanding of the associated particle acceleration process. Depending on the plasma properties of interest, different means of plasma probing are necessary, such as charged particle pulses to access the sheath structure and the electromagnetic fields of a plasma [1] or X-ray Thomson scattering to measure the electron temperature $T_e$ and deduce the electron density $n_e$ [2]. In this paper, however, we report on experiments where the probing is carried out with an ultrashort optical laser pulse, which offers the possibility to directly image the evolution of the plasma's density distribution from which its expansion velocity can be retrieved. The used targets are water micro-droplets. In contrast to experiments with thin foils [3], the spherical symmetry and limited extension of droplets in all spatial directions facilitates a direct and mostly unobstructed imaging of the plasma expansion process using shadowgraphy. Furthermore, foils have to be replaced by a fresh target after each shot [4], whereas microdroplets are a cost-effective alternative and can be used with high repetition rates.

 

Journal of Physics: Conference Series **3124** (2025) 012022 doi:10.1088/1742-6596/3124/1/012022

## 2. Experimental setup

The experiment was conducted at the POLARIS laser system [5] at the Institute of Optics and Quantum Electronics at the Friedrich-Schiller-University Jena and the Helmholtz-Institute Jena. The target consisted of water micro-droplets of 20 µm in diameter. The droplets were generated using a jet of water produced by a commercial nozzle (Micro Jet Components). The latter was driven by a piezo motor to break up the jet, forming droplets at a high repetition rate (1.2 MHz). The POLARIS pump laser pulses (1030 nm, 100 TW) were focused onto the water droplets (focal spot area $A \approx 20\,\mu\text{m}^2$) to intensities of $I_\text{L} \approx 4 \times 10^{19}\,\text{W}\,\text{cm}^{-2}$. The experimental setup with the main components is shown in Fig. 1.

The probing system [6] utilized a single pass non-collinear optical parametric amplifier (NOPA) with a µJ-level probe energy and a broad bandwidth between 750 nm to 950 nm. The probe pulses were first sent through a delay stage (1), which was used to change the temporal delay between the main pulse and the probe pulse with a sub-picosecond accuracy. Then, the probe light was slightly focused using a lens in order to illuminate the whole interaction region with sufficient probe-light intensity. The imaging was realized with a magnifying microscope objective (8) Mitutoyo Plan Apo NIR 10x, which collimated the light from the droplet position, and a 400 mm tube lens that finally imaged the interaction region onto the two cameras labeled *probe 1* and *probe 2*. To minimize the reflection of the p-polarized pump's stray light (the probe light was rotated to s-polarization using a half wave plate), the glass plates (4) and (5) were inserted at the Brewster angle $\varphi_B = 55.5°$ (at 800 nm). However, this only partly reduces the unpolarized part of the plasma emission in the center of the droplet. Additionally, the complete broadband emission of the plasma cannot be completely filtered with a bandpass filter.

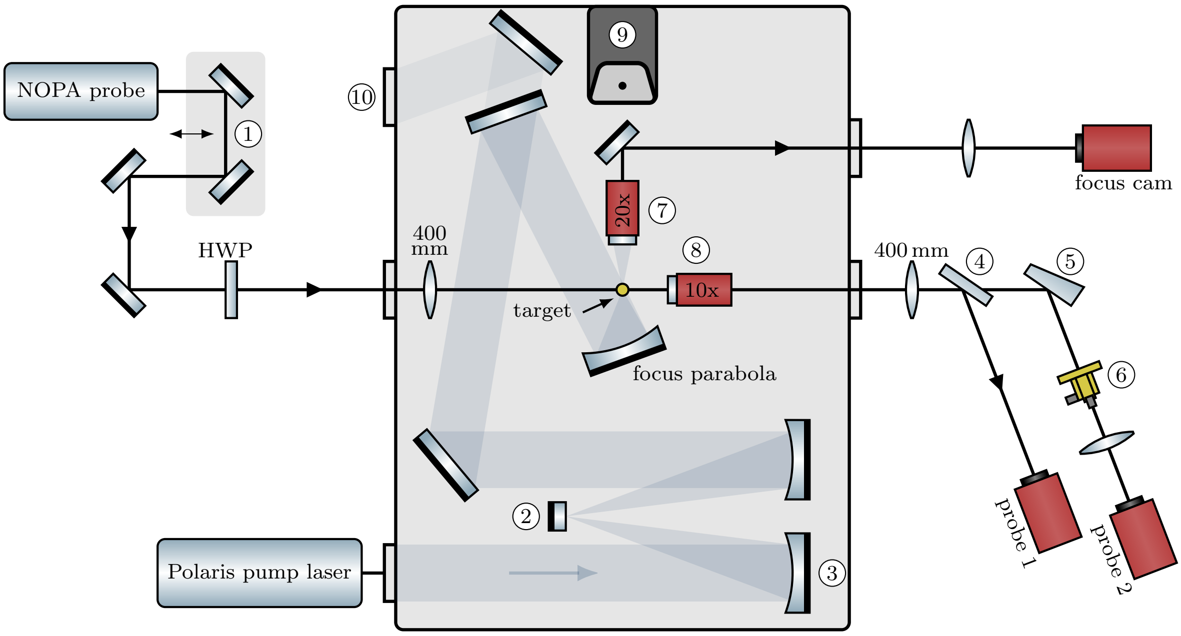


**Figure 1.** Experimental setup (not to scale) of the laser-matter interaction and the imaging system of the probe. (1) delay stage for pump-probe synchronization and delay variations, (2) plasma mirror, (3) off-axis parabola, (4) thin glass plate used for splitting the beam, (5) wedged glass plate, (6) coronagraph (c. f. section 3), (7) focus objective, (8) probe objective with bandpass filter 800 nm (40 nm FWHM), (9) ion diagnostics, (10) beam towards plasma mirror diagnostics and online pump pulse near- and far-field diagnostics.

## 3. Plasma emission suppression with a coronagraph

The interaction of the main pulse with the droplets leads to a strong emission of electromagnetic radiation from the generated plasma, with one particular important process being resonance absorption that produces the second harmonic of the pump laser pulse [7]. More processes [7, 8] may induce unpolarized, broadband emission of the plasma which cannot entirely be filtered by a bandpass filters or by polarization control. However, the emission is restricted to the size of the droplet. A mask is used at an intermediate image plane to block the central part of the droplet, from which the bright plasma emission originates. The concept comes from a coronagraph [9], which is used to image the corona of the sun while blocking the sun's direct light that would otherwise saturate or damage the detector. For the setup we used a filter wheel into which individual filter holders carrying appropriate masks could be screwed (c. f. Fig. 2 left). With the help of stepper motors, the position of the filter wheel and therefore also the mask can be controlled in three dimensions. The droplets are imaged simultaneously onto the cameras with *probe 1* using only spectral and polarization filtering, and *probe 2* using the coronagraph as well.

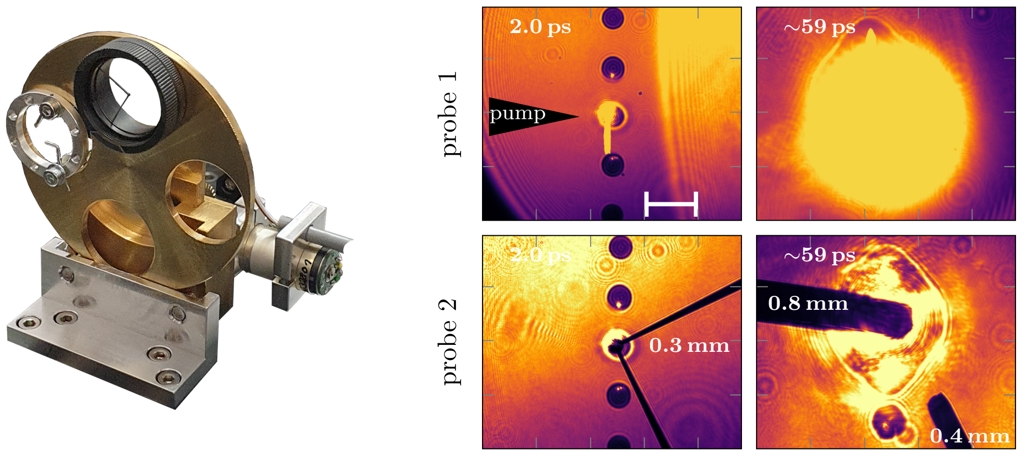


**Figure 2.** Left: Filter wheel containing individual filter holders carry masks of different sizes and shapes. Right: Comparison of *probe 1* (top) and *probe 2* (bottom) images for different probe-pump delays. The scale in the top left image corresponds to 50 µm in the droplet plane (same scale in all images). The lengths indicate the diameter of the masks. The plasma emission saturates the *probe 1* camera which creates pixel errors or conceals the whole expansion region.

## 4. Shadowgraphy of the plasma evolution

The temporal evolution of the plasma expansion was observed by changing the delay between pump and probe pulse using the delay stage (1) in Fig. 1. The delay can be adjusted in time steps of less than 100 fs, however, we estimated the temporal jitter between the probe pulse and the main pulse to be 400 fs. Furthermore, the temporal evolution of the plasma expansion can only be reliably deduced from subsequently recorded images (different relative delays) under the assumption that the laser-plasma interactions in the different shots are sufficiently comparable.

The whole plasma expansion process was probed in a time interval of $\tau = -4.7$ ps to 258 ps, where $\tau$ denotes the temporal delay between pump and probe pulse. Negative values indicate that the probe pulse arrived first. For $\tau \geq -1$ ps the coronagraph was inserted. The expansion is shown via a collection of shadowgrams recorded by *probe 2* (c. f. Fig. 3). The individual pump-probe delays for each shadowgram are denoted in the upper left corner with an uncertainty of $\pm 1$ ps. This is due to an uncertainty in determining the zero delay point and the temporal jitter between pump and probe pulse.

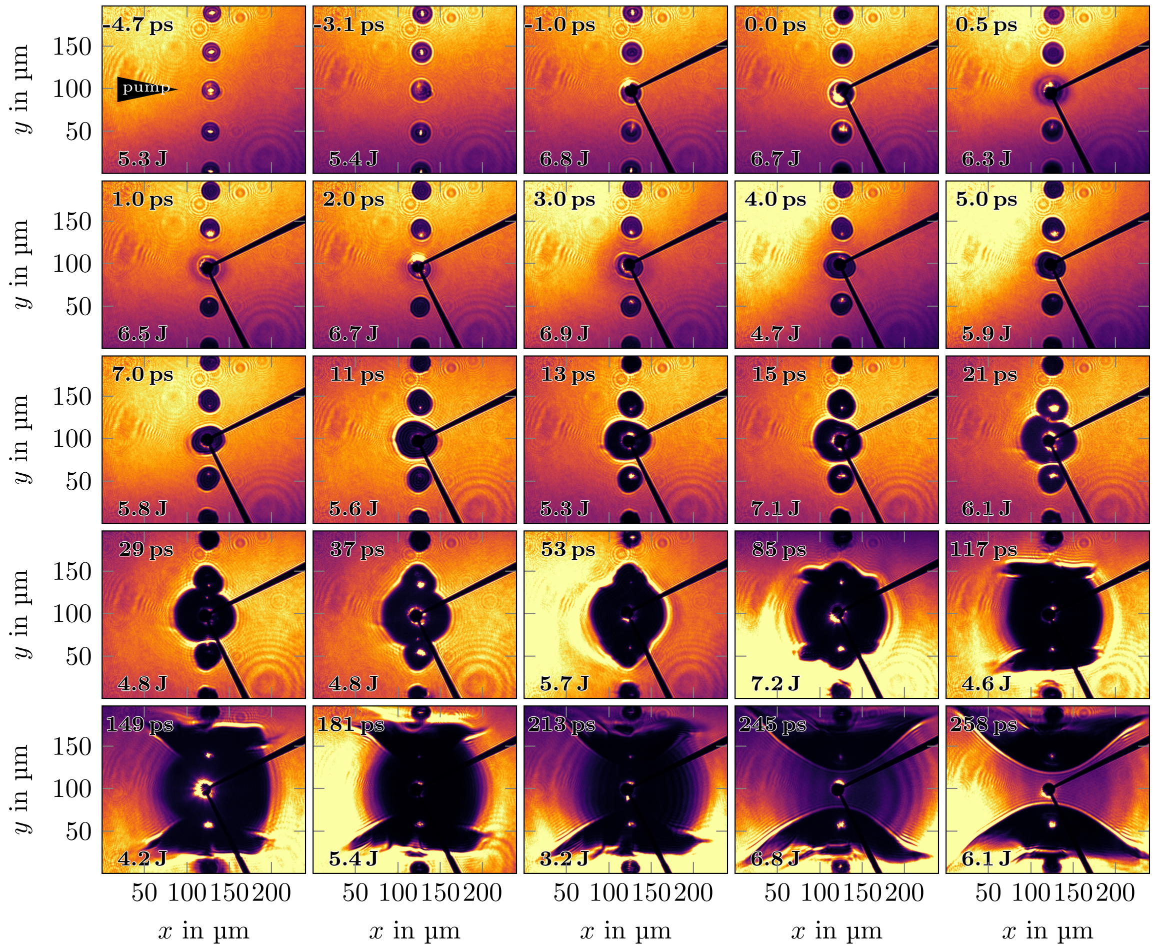


**Figure 3.** Images of the water droplets recorded with the camera *probe 2* (for $\tau \geq -1\,\text{ps}$ with the coronagraph in place). The main pulse's laser energy on target (for all shots) ranged between 3.2 J to 8.0 J with a mean value of $E = 6.1(9)\,\text{J}$ (standard variation).

For the determination of the absolute time delay of the shots with respect to the peak of the pump laser pulse, we examined the change of opacity of the droplets due to ionization for different delays. In fact, when the rising edge of the main pulse arrives, a blackening of the central droplet's image can be observed, because the pulse ionizes this droplet and generates a plasma with an overcritical density ($n_{\text{cr}} = 1.74 \times 10^{21}\,\text{cm}^{-3}$ is the critical density calculated at 800 nm), through which the probe can no longer propagate. At slightly later times, the first and second neighbours of the central droplet start blackening too. This point is identified as the *zero delay* point, where the probe pulse and the peak of the pump laser pulse coincide. The outer areas of the focus are much less intense at the periphery than in the centre of the focus, i. e. an ionization process in the neighbouring droplets can only be triggered at the time of the peak of the main pulse. Note that this interpretation of the zero delay point is ambiguous, as the rising edge of the pulse may also cause the droplets to become opaque.

For increasing delays of the probe, the spatial extent of the dark volume of overcritical plasma also increases. The created plasma will either lead to absorption of the probe light in the dark region or to reflection or refraction of the probe light out of the collecting aperture of the microscope objective. From the shadowgraphy images, the expansion of the plasma's critical density front can be estimated by measuring the size of the shadow as shown in Fig. 4 (bottom).

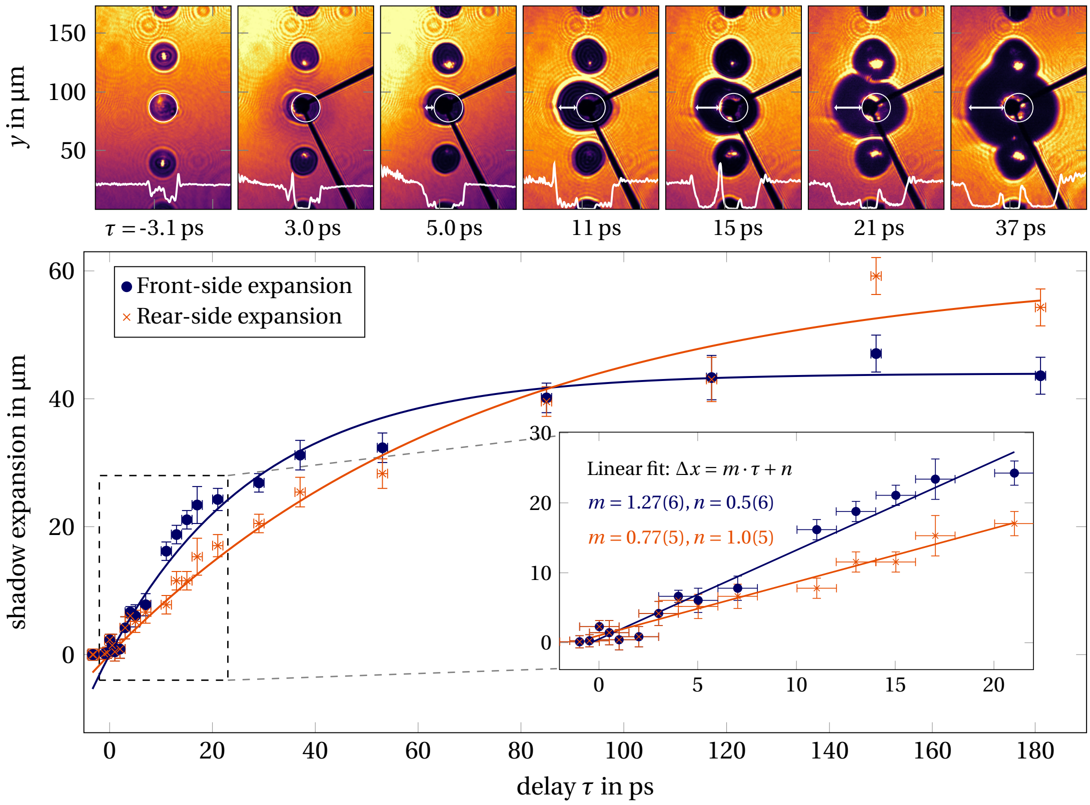


**Figure 4.** Top: Images of the plasma expansion for different delays $\tau$. The white arrows denote the measured plasma expansion from the original position and size of the central droplet (white circles) which was obtained from horizontal lineouts. Bottom: Expansion of the front (blue) and rear (orange) of the plasma parallel to the laser propagation axis plotted as a function of temporal delay $\tau = t - t_0$ of the probe with respect to the pump laser pulse arriving at $t_0$. The solid curves are exponential fits to the front and rear-side expansion. Inset: Same image emphasizing the short time scales of $\tau < 20\,\text{ps}$ (dashed rectangle) in a linear expansion regime.

The error-bars result from the limited spatial resolution and the faint transition between shadow and background illumination. After $\tau \approx 3\,\text{ps}$, a rapid growth of the shadow can be observed, where the front side expands faster than the rear side. In this regime the plasma expansion mainly occurs along the laser axis and is linear. The linear fits (c. f. fig.4 bottom) yield the following velocities

$$\tau = 3\,\text{ps to } 20\,\text{ps} \qquad v_{\text{front}} = 1.27(6)\,\text{µm}\,\text{ps}^{-1}, \quad v_{\text{rear}} = 0.77(5)\,\text{µm}\,\text{ps}^{-1} \tag{1}$$

$$\tau = 80\,\text{ps to } 190\,\text{ps} \qquad v_{\text{front}} = 0.09(3)\,\text{µm}\,\text{ps}^{-1}, \quad v_{\text{rear}} = 0.22(5)\,\text{µm}\,\text{ps}^{-1}. \tag{2}$$

For longer delays the plasma starts to expand spherically outward, which geometrically results in a smaller expansion velocity when measured in one fixed direction. This is illustrated by exponential fits represented by the solid lines in Fig. 4. Additionally, as the heating source (pump laser beam) of the plasma is already gone, the electron temperature and thus the expansion velocity are further reduced. For small delays the experimental results are comparable to similar shadowgraphy experiments with liquid targets (c. f. Tab. 1).

From the expansion velocity, the ion sound speed can be estimated. Assuming that eight of the total of ten electrons per water molecule are freed (the Over-the-Barrier Ionization

Journal of Physics: Conference Series **3124** (2025) 012022 doi:10.1088/1742-6596/3124/1/012022

**Table 1.** Comparison of shadowgraphic plasma expansion experiments with targets for different intensities. The relevant parameters are the laser intensity $I_L$ and wavelength $\lambda$.

| experiment | target | intensity $I_L$ | $\lambda$ | $v_{\text{front}}$ |
|---|---|---|---|---|
| Becker [10, 11, p. 77] | water droplets | $10^{16}\,\text{W}\,\text{cm}^{-2}$ | 400 nm | $0.38\,\mu\text{m}\,\text{ps}^{-1}$ |
| This thesis | water droplets | $4 \times 10^{19}\,\text{W}\,\text{cm}^{-2}$ | 1030 nm | $1.3\,\mu\text{m}\,\text{ps}^{-1}$ |
| Bernert et al. [12] | hydrogen jet | $5.4 \times 10^{21}\,\text{W}\,\text{cm}^{-2}$ | 800 nm | $23\,\mu\text{m}\,\text{ps}^{-1}$ |

threshold of the last two charge states is above $10^{19}\,\text{W}\,\text{cm}^{-2}$), the maximum electron density is $n_{e,0} = 8\frac{\varrho}{M}N_A = 153 n_{\text{cr}}$ at $\lambda = 0.8\,\mu\text{m}$, where $M = 18.02\,\text{g}\,\text{mol}^{-1}$ is the molar mass of water, $\varrho$ its density and $N_A$ Avogadro's constant. The front of the expansion $x_{\text{front}}$ is assumed to have a density of $n_{\text{cr}}$. In a simple model, assuming an exponential plasma electron density distribution, the ion sound speed of the front can be estimated as

$$n_e(x_{\text{front}}, t) = n_{e0} \exp\left(-\frac{x_{\text{front}}}{c_s t}\right) \quad \Rightarrow c_s = \underbrace{\frac{x_{\text{front}}}{t}}_{v_{\text{front}}} \frac{1}{\ln(n_{e0}/n_{\text{cr}})} = 0.25\,\frac{\mu\text{m}}{\text{ps}}. \tag{3}$$

This value can be compared to a theoretical estimation of the ion sound velocity of the generated plasma. The ion sound velocity depends on the electron temperature $T_e$ (also the ion mass $m_i$ and the charge state $Z$), which can be calculated by the ponderomotive scaling model for hot electrons [13]

$$c_s = \sqrt{\frac{k_B T_e Z}{m_i}} \quad \text{and} \quad k_B T_e = m_e c^2(\bar{\gamma} - 1) \quad \text{with} \quad \bar{\gamma} = \sqrt{1 + \frac{I_L \lambda_L^2}{1.37 \cdot 10^{18}} \frac{\text{cm}^2}{\text{W}\,\mu\text{m}^2}}. \tag{4}$$

$\bar{\gamma}$ is the cycle-averaged relativistic Lorentz factor, which depends on the laser intensity $I_L$ and wavelength $\lambda_L$. For the intensity $I_L \approx 4 \times 10^{19}\,\text{W}\,\text{cm}^{-2}$ and a wavelength $\lambda_L = 1030\,\text{nm}$, the kinetic energy of the electrons is $k_B T_e \approx 2.4\,\text{MeV}$. For a hydrogen plasma, the ion sound speed is then determined to be $c_s \approx 15\,\mu\text{m}\,\text{ps}^{-1}$. For $O_6^+$, however, the ion sound speed is reduced to $9\,\mu\text{m}\,\text{ps}^{-1}$.

The theoretical estimation and experimental value differ by a factor of almost 40. However, the electron thermal energy was calculated only for *hot electrons*. Furthermore, the plasma expansion model is an isothermal model of a planar plasma with a constant density ($n_{e0}$) in the central region. For large delays $\tau \approx 240\,\text{ps}$, the target center becomes transparent which invalidates this assumption, as the plasma becomes underdense. Additionally, with the formation of a pre-plasma by the rising edge of the pulse, the absorption mechanism might be different and the electron temperature scaling may change. Moreover, measurements of the hot electron energy distributions in solid targets revealed a resonance absorption scaling of $k_B T \propto (I\lambda^2)^{1/3}$ in a range of $10^{18}\,\text{W/cm}^2\mu\text{m}^2$ to $10^{21}\,\text{W/cm}^2\mu\text{m}^2$ [14, 15], which would cause the calculated ion sound speed to be further reduced.

## 5. Conclusion

In a high-intensity, relativistic laser-plasma experiment using water micro-droplets as the target, we used an off-harmonic pump-probe setup to study the temporal evolution of the created plasma. We illuminated the droplets and the interaction region with the probe pulse and recorded shadowgraphic images for different delays between the probe and main pulse. In order to suppress the strong emission of the plasma, we incorporated different filtering techniques, such as a spectral bandpass filter, glass plates inserted under the Brewster angle to mitigate p-polarized stray light from the pump laser, and a coronagraph. The latter was an opaque mask blocking the center of the droplet in an intermediate image plane. We measured the evolution of the plasma expansion up to delays of 200 ps. In a range of 3 ps to 20 ps after the arrival of the main pulse, the plasma expansion was approximately linear with an expansion velocity of the plasma front $v_{\mathrm{front}} = 1.3 \times 10^6\,\mathrm{m\,s^{-1}}$ which is comparable to similar liquid target experiments. Additionally, the plasma expansion is observed to behave differently at the front and the rear side of the droplet. An estimation of the ion sound velocity was performed with a simple plasma expansion model and the calculated density of the central plasma. These values were compared to theoretical calculations using the ponderomotive scaling for hot electrons. This model, however, could not reproduce the measured values of the ion sound velocity in our interaction configuration, possibly due to simplified assumptions of the expansion model or the existance of different electron temperature scaling laws at these intensities and for our experimental conditions.

**Acknowledgement**
The authors are grateful for support from the European Union's Horizon 2020 Research and Innovation programme under Grant Agreement No 101004730.

## References

[1] Carstensen J, Haase F, Jung H, Tadsen B, Groth S, Greiner F and Piel A 2013 *IEEE Transactions on Plasma Science* **41** 764–768
[2] Urry M, Gregori G, Landen O, Pak A and Glenzer S 2006 *Journal of Quantitative Spectroscopy and Radiative Transfer* **99** 636–648 ISSN 0022-4073 radiative Properties of Hot Dense Matter
[3] Jäckel O, Polz J, Pfotenhauer S, Schlenvoigt H, Schwoerer H and Kaluza M 2010 *New Journal of Physics* **12** 103027
[4] Gao Y, Bin J, Haffa D, Kreuzer C, Hartmann J, Speicher M, Lindner F H, Ostermayr T M, Hilz P, Rösch T F and et al 2017 *High Power Laser Science and Engineering* **5** e12
[5] Hornung M, Liebetrau H, Keppler S, Kessler A, Hellwing M, Schorcht F, Becker G A, Reuter M, Polz J, Körner J, Hein J and Kaluza M C 2016 *Opt. Lett.* **41** 5413–5416
[6] Tamer I, Hellwing M, Azamoum Y, Hornung M, Keppler S, Schorcht F, Hein J and Kaluza M C 2020 *Opt. Express* **28** 19034–19043
[7] Teubner U and Gibbon P 2009 *Rev. Mod. Phys.* **81**(2) 445–479
[8] Bobin J L 1985 *Physics Reports* **122** 173–274
[9] Lyot B 1939 *Monthly Notices of the Royal Astronomical Society* **99** 580
[10] Becker G A, Schwab M B, Lötzsch R, Tietze S, Klöpfel D, Rehwald M, Schlenvoigt H P, Sävert A, Schramm U, Zepf M *et al.* 2019 *Scientific reports* **9** 1–8
[11] Becker G 2021 *Characterization of laser-driven proton acceleration with contrast-enhanced laser pulses* Ph.D. thesis
[12] Bernert C, Assenbaum S, Brack F E, Cowan T E, Curry C B, Garten M, Gaus L, Gauthier M, Göde S, Goethel I *et al.* 2022 *Scientific reports* **12** 1–11
[13] Wilks S C, Kruer W L, Tabak M and Langdon A B 1992 *Phys. Rev. Lett.* **69**(9) 1383–1386
[14] Beg F, Bell A, Dangor A, Danson C, Fews A, Glinsky M, Hammel B, Lee P, Norreys P and Tatarakis M 1997 *Physics of plasmas* **4** 447–457
[15] Chen H, Wilks S C, Kruer W L, Patel P and Shepherd R 2009 *Physics of plasmas* **16** 020705